

## Experimental Benchmark for an Improved Simulation of Absolute Soft-X-Ray Emission from Polystyrene Targets Irradiated with the Nike Laser

J. L. Weaver,<sup>1</sup> M. Busquet,<sup>2</sup> D. G. Colombant,<sup>1</sup> A. N. Mostovych,<sup>1</sup> U. Feldman,<sup>2</sup> M. Klapisch,<sup>2</sup> J. F. Seely,<sup>3</sup> C. Brown,<sup>3</sup> and G. Holland<sup>4</sup>

<sup>1</sup>Plasma Physics Division, U.S. Naval Research Laboratory, Washington, D.C. 20375, USA

<sup>2</sup>ARTEP, Inc., Ellicott City, Maryland 21042, USA

<sup>3</sup>Space Science Division, U.S. Naval Research Laboratory, Washington, D.C. 20375, USA

<sup>4</sup>SFA, Inc., Landover, Maryland 20785, USA

(Received 22 October 2004; published 3 February 2005; corrected 23 February 2005)

Absolutely calibrated, time-resolved spectral intensity measurements of soft-x-ray emission ( $h\nu \sim 0.1\text{--}1.0$  keV) from laser-irradiated polystyrene targets are compared to radiation-hydrodynamic simulations that include our new postprocessor, Virtual Spectro. This new capability allows a unified, detailed treatment of atomic physics and radiative transfer in nonlocal thermodynamic equilibrium conditions for simple spectra from low- $Z$  materials as well as complex spectra from high- $Z$  materials. The excellent agreement (within a factor of  $\sim 1.5$ ) demonstrates the powerful predictive capability of the codes for the complex conditions in the ablating plasma. A comparison to data with high spectral resolution ( $E/\delta E \sim 1000$ ) emphasizes the importance of including radiation coupling in the quantitative simulation of emission spectra.

DOI: 10.1103/PhysRevLett.94.045002

PACS numbers: 52.25.Os, 32.70.Fw, 52.38.Ph, 52.65.Ww

The knowledge of absolute intensity of extreme UV (XUV) and x-ray radiation created by the laser irradiation of solid targets is crucial for issues in inertial confinement fusion (ICF) ranging from illumination sources for back lighter diagnostics [1] to efficient sources to drive implosions [2]. The correct estimation of the role of radiation transfer in the evolution of the plasma depends in a large measure on the intensity of the emitted radiation. This is especially true for indirect-drive ICF which utilizes an envelope, or hohlraum, around the fuel pellet to convert laser light into smoothed XUV radiation which ablates and implodes the pellet. Typically, hohlraums are made from Au and, accordingly, the absolute XUV emission from laser-irradiated Au has been studied extensively [3]. However, most pellet designs, whether for indirect-drive or direct-drive ICF, incorporate a polystyrene (CH) shell to contain the DT fuel. This central role of CH means that a comparison of *absolute* measurements of its intensity from a laser target with simulations of *absolute* emissivity is vital. Numerous spectroscopic studies of laser-irradiated low- $Z$  targets such as CH have been published [4] but, to the best of our knowledge, an experimentally benchmarked prediction of absolutely calibrated, spectrally resolved emission from CH, relevant to ICF purposes, has not been published. In this Letter, we compare the emission from planar CH targets measured with absolutely calibrated transmission grating spectrometers to simulations performed with a new postprocessor [Virtual Spectro (VS)]. We report agreement between the predicted and measured values for the absolute intensity better than a factor of  $\sim 1.5$  in the soft-x-ray region ( $h\nu \sim 0.1\text{--}1.0$  keV). This agreement provides confidence in the radiation-hydrodynamic simulations used at the U.S. Naval Research Laboratory (NRL) for ICF pellet design, in which

the opacities are calculated by the supertransition arrays (STA) model [5] and the non-LTE (local thermodynamic equilibrium) effects are treated with the RADIOM [6] model. The postprocessor VS goes beyond STA and LTE approximations; it is a detailed fine-structure radiative collisional model with radiation coupling.

Absolute comparisons of spectral intensities are seldom made, because they are difficult. On the experimental side, everything has to be calibrated: the laser irradiance, on the targets, all the components of the spectrometers—slits, filters, gratings, detectors, etc.—as well as geometrical factors, such as solid angles and distances. On the theoretical side, the spatial and temporal histories of temperature and density of the plasma need to be accurately reproduced, reliable atomic physics models are necessary for the population of the emitting energy levels and for transition probabilities, and radiative transfer and coupling to the various atomic species has to be taken into account.

Radiation-hydrodynamic simulations of laser-irradiated targets must include a large number of phenomena to provide reliable descriptions of experimental conditions. Work at NRL has focused on developing a code suite to analyze direct-drive schemes for ICF. The hydrodynamic code, FAST [7], is a multidimensional code which has been parallelized to enable faster operation for 2D or 3D runs. It uses flux corrected transport [8] to provide a highly sophisticated adaptive gridding algorithm that efficiently captures the sharp gradients inherent in these physical systems. FAST works with the quasineutral approximation to treat the plasma as a single fluid, although distinct electron and ion temperatures can be maintained in the runs. Laser absorption is described by inverse bremsstrahlung with induced spatial incoherence smoothing (ISI). Electron thermal conduction follows the classical flux

limited Spitzer-Harm model with quantum corrected conductivity [9]. The various equations of state for the target materials are tabulated, and a multigroup radiation diffusion model with a variable Eddington factor is used for radiation transport [7]. The necessary opacities are interpolated for each cell from tables calculated off-line for a dense grid of values for temperature, density, and photon energy. In the present case, these tables were obtained with the STA model in (LTE), and corrected for non-LTE effects with the RADIOM model. FAST can also use tables from SCROLL [10], a non-LTE version of STA, but this was not necessary for this Letter, due to the relatively low emissivity of CH. The FAST code has been successfully tested against primarily hydrodynamic effects (e.g., Rayleigh-Taylor instability growth [11] and Richtmyer-Meshkov instabilities [12]). Now detailed predictions for radiation effects [13] have required development of a new postprocessor.

Like FLY [14] or TRANSPEC [15], Virtual Spectro [16] is a postprocessor which uses temperatures, densities, average charge state, and velocities as a function of time and position as computed by a 1D or 2D hydrodynamic code. The hydrodynamic code dumps from FAST can be given in either Lagrangian mode, Eulerian, or arbitrary Lagrangian-Eulerian (ALE) mode. VS can process a pure material or each component of a compound. First, using the mass density and electron temperature for each cell, VS computes the relevant specific electron density for the simulation. The atomic structure data (taken from published values or computed with the HULLAC [10] code suite) is then used to compute time dependent atomic populations, outgoing flux ( $J_\nu$ ), and opacity ( $K_\nu$ ) with a second order advection scheme in the non-ALE mode, though it has been checked that the quasisteady state approximation is valid for the present study. Radiation transport in resonance lines, taking into account line broadening, is coupled to kinetic equations using a mix of the accelerated lambda iteration scheme and the partial linearization method; see Fig. 1. The final outputs are used to create synthetic spectra with temporal, spatial, and energy resolution where opacity effects are accurately accounted for. The experimental setup (including integration along the line of sight at a particular view angle, instrumental spectral resolution, and time integration) can be incorporated in the final output spectra.

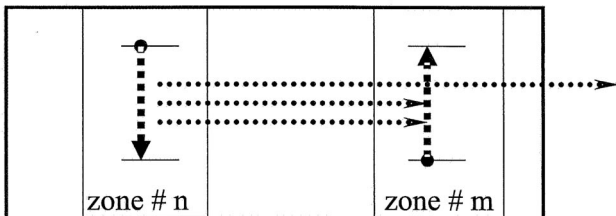


FIG. 1. Radiation trapping—between different zones—increases excited state populations (thus local emissivity) but decreases the outgoing x-ray flux.

Experiments to test the predictions of FAST and VS were carried out at the Nike laser facility. The Nike laser [17] is a high power ( $\sim 10^{14}$  W cm $^{-2}$ ) KrF system. Nike operates at 248 nm, has a relatively large bandwidth (1–2 THz), and provides very uniform beam intensity profiles ( $\delta I/I < 0.2\%$ ) on a 500  $\mu$ m focal spot due to the use of the ISI smoothing technique [18]. For the results in this Letter, standard 40  $\mu$ m thick planar CH targets were placed at the target chamber center and irradiated with a 3.5 ns pulse at an incident power density of  $1.13 \times 10^{13}$  W cm $^{-2}$ . The prepulse intensity was less than a factor of  $10^{-4}$  below the level of the main pulse. The normal to the target surface was aligned along the average laser propagation direction for the laser beams.

Soft x rays emitted from the target plasma were recorded with two transmission grating spectrometers (TGS) and a grazing incidence spectrometer (GIS). These TGS were installed to view the target at two widely separated viewing angles to determine the angular dependence of the soft-x-ray emission. The “normal” viewing spectrometer had a line of sight at an angle of  $14^\circ$  to the target normal and the “wide” viewing spectrometer had a line of sight at  $42^\circ$  to target normal. The TGS provided time-integrated and time-resolved spectra ( $\delta t \sim 0.3$  ns) with moderate spectral resolution ( $\delta\lambda/\lambda \sim 10$ –20) and accurate determination ( $\sigma_I/I < 15\%$ ) of the intensity (W ster $^{-1}$ ). The main optical elements of both TGS were a 2500 1/mm gold transmission grating, an adjustable entrance slit, a freestanding 1800  $\text{\AA}$  thick Al foil transmission filter, a Si photodiode array, and a phosphor-coupled charge coupled device camera. The sensitivity calibrations of the transmission filters, transmission gratings, and photodiode arrays were performed at the X24C beam line of the National Synchrotron Light Source at Brookhaven National Laboratories [19].

In this Letter, we show only results from the normal viewing spectrometer due to its higher spectral resolution and because its line of sight is more closely aligned to the target normal. Observations that included the wider viewing spectrometer verified that the variation of absolute intensity with view angle is not significant for the slight off-normal view angles in the case of CH targets.

The GIS provided high spectral resolution ( $\delta\lambda/\lambda \sim 1000$ ) but was time integrated and not absolutely calibrated. The GIS included a cylindrically curved focusing mirror, a 40  $\mu$ m wide entrance slit, a 1200 1/mm gold coated concave grating with a  $2^\circ$  blaze angle, and a 3 m radius of curvature [20]. Time-integrated spectra were recorded with glass photographic plates. We calibrated the intensity response of the film plates from the ratio of the line intensities using the standard procedure of multiple shot exposures. The grazing incidence spectrometer viewed the target at an angle of  $42^\circ$ . The spatial resolution across the target at the photographic plate was  $\sim 50$   $\mu$ m/mm.

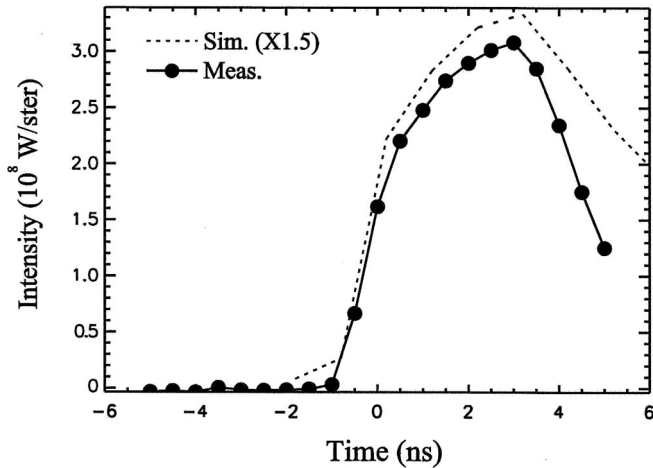


FIG. 2. Spectrally integrated, time-resolved data. Comparison of output from Virtual Spectro (dashed line) and from the absolutely calibrated transmission grating spectrometer (solid line and closed circle). The simulated spectral intensity was multiplied by 1.5.

We have postprocessed hydrodynamic simulations computed in the one dimensional mode of FAST (FAST1D) using 400 spatial cells and 98 nonequidistant energy groups to provide adequate resolution of the carbon lines while allowing tractable computation times. The laser pulse time history and peak intensity ( $1.13 \times 10^{13} \text{ W cm}^{-2}$ ) were taken from the laser diagnostics for the observed shots. The FAST output was collected at 80 dump times. In VS, the atomic structure was taken from the literature for H-like and He-like resonant lines and for satellites of  $\alpha$  and  $\beta$  lines [21]. In all ions, hydrogenic levels have been added to complement the database up to  $n = 15$ . Stark broadened line profiles using tabulated microfield distribution were used for the resonant lines up to  $n = 4$  [22]. As mentioned previously, only resonant lines were considered here due to the comparatively low intensity for the satellite lines. For the comparison with experiment, the synthetic spectra are convolved with (Gaussian) instrumental functions of widths appropriate for each instrument.

Normal incidence synthetic spectra in the range 250–600 eV and time- or spectral-integrated values are compared to the absolute intensity measurement. Figure 2 demonstrates that the simulation reproduces correctly the rise of the emission. Note that the simulations in both Figs. 2 and 3 are multiplied by a factor of 1.5 to emphasize the agreement on the shapes. After the laser pulse ends, the simulation has a slower decay of the emission compared to the measurements. This may be due to 2D cooling effects not included in the 1D simulation. Figure 3 compares the observed values for the absolute time-integrated spectral intensity ( $\text{J/ster}/\text{\AA}$ ) to the final output from VS. The two *absolute* spectra agree very well. There is an apparent wavelength shift of the satellite lines at 38  $\text{\AA}$ . Several lines are blended there due to the poor resolution. A slight error in the temperature during the plasma expansion after the

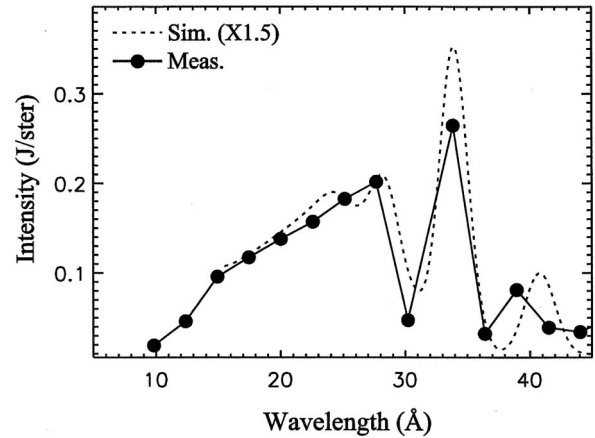


FIG. 3. Time-integrated, spectrally resolved data. Comparison of output from Virtual Spectro (dashed line) and from the absolutely calibrated transmission grating spectrometer (solid line and closed circle). The simulated spectral intensity was multiplied by 1.5.

laser pulse could change the intensity ratios and cause this apparent shift. The  $\sim 25\%$  discrepancy in the intensity ratio of He-like to H-like emission may also be due to such an error.

Figures 4 and 5 compare a high-resolution time-integrated spectrum recorded on film by the GIS with corresponding VS results. They also show simulations, with and without coupling to the radiation field, of the level populations up to  $n = 4$  for hydrogenlike and heliumlike carbon. All spectra in both figures have been normalized to the peak of the  $\text{Ly}\beta$  line. It can be seen that the inclusion of line coupling for computation of populations causes a dramatic change in the simulated spectra. The unobserved features around 27  $\text{\AA}$  of Fig. 4 disappeared,

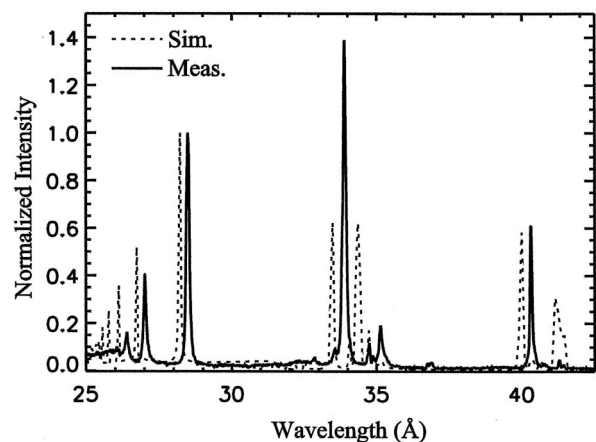


FIG. 4. Time-integrated spectrum. The comparison of simulation *without* coupling between resonant lines (dashed line) to the high-resolution spectrum from the grazing incidence spectrometer (solid line) shows an overestimate of the intensities of many spectral lines, particularly satellite lines. Each spectrum has been normalized to the  $\text{Ly}\beta$  intensity of hydrogenlike carbon.

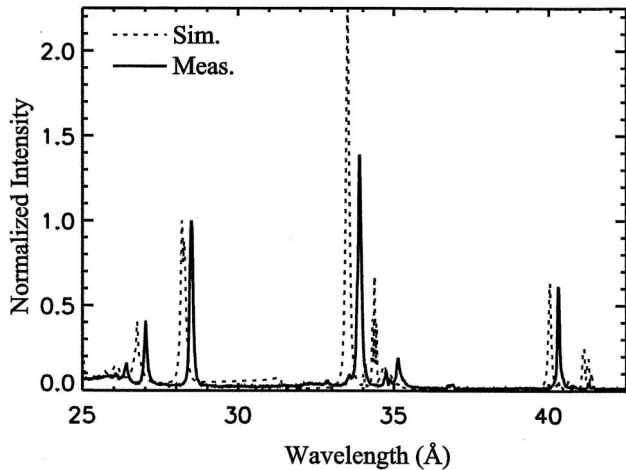


FIG. 5. Time-integrated spectrum. The comparison of simulation *with* coupling between resonant lines (dashed line) to the high-resolution spectrum from the grazing incidence spectrometer (solid line) shows an improved estimation of the intensities. Each spectrum has been normalized to the Ly $\beta$  intensity of hydrogenlike carbon.

and the ones at 34 and 42 Å are much smaller, although still present. Also the level of the continuum below 26 Å agrees better. Most of the remaining discrepancies are in the line intensity ratios, which depend on the relative abundances of the H-like and He-like ions. These differences can be attributed to slight errors in the simulated temperatures from FAST, or to transitions in the free-bound continuum not coupled through photoionization, or to the limitations of the atomic model. It is clear, however, that radiation transport and coupling in the rate equations of atomic levels play an important role.

All in all, the agreement between simulation and experiment shown in Figs. 2 and 3 is remarkable, in view of the difficulty of the calibration, and the complexity of the simulation. This has important implications: because the underlying data for Virtual Spectro is the output from the FASTID code, the success of the final product implies that the radiation hydrodynamics code suite is predicting the temperature and density of the emission region accurately. The radiation present in the physical system does not dominate the evolution of the system. The STA tables and RADIOM models provide fairly good accuracy, although not the detailed spectral information created by Virtual Spectro. These new results represent a significant advance in the ability to accurately describe conditions in laser-irradiated targets. We plan to address the comparison of spectra of high-Z elements, which is much more difficult, in the near future.

This work was supported by the U.S. Department of Energy.

- [1] D.L. Matthews *et al.*, J. Appl. Phys. **54**, 4260 (1983); M.H. Key *et al.*, Phys. Rev. Lett. **41**, 1467 (1978).
- [2] See *Laser Interactions and Related Plasma Phenomena*, edited by G.H. Miley and H. Hora (Plenum, New York, 1992), Vol. 20.
- [3] D.R. Kania *et al.*, Phys. Rev. A **46**, 7853 (1992); P.D. Goldstone *et al.*, Phys. Rev. Lett. **59**, 56 (1987); W.C. Mead *et al.*, Phys. Fluids **26**, 2316 (1983); H. Nishimura *et al.*, Phys. Rev. A **43**, 3073 (1991); T. Mochizuki *et al.*, Phys. Rev. A **33**, 525 (1986).
- [4] B.C. Boland *et al.*, J. Phys. B **2**, 1180 (1968); F.E. Irons and N.J. Peacock, J. Phys. E **6**, 857 (1973); P.T. Rumsby, J.W.M. Paul, Plasma Phys. **16**, 247 (1974); M. Galanti and N.J. Peacock, J. Phys. B **8**, 2427 (1975); J.F. Seely *et al.*, Phys. Rev. A **23**, 1437 (1981); W.C. Mead *et al.*, Phys. Rev. Lett. **47**, 1289 (1981); K. Eidmann and T. Kishimoto, Appl. Phys. Lett. **49**, 377 (1986); P.D. Gupta *et al.*, Phys. Rev. A **33**, 3531 (1986); R. Popil *et al.*, Phys. Rev. A **35**, 3874 (1987); Y. Y. Tsui *et al.*, Phys. Fluids B **5**, 4115 (1993).
- [5] A. Bar-Shalom *et al.*, Phys. Rev. A **40**, 3183 (1989); A. Bar-Shalom *et al.*, Phys. Rev. E **59**, 3512 (1999).
- [6] M. Busquet, Phys. Fluids B **5**, 4191 (1993).
- [7] J.H. Gardner *et al.*, Phys. Plasmas **5**, 1935 (1998).
- [8] J.P. Boris and D.L. Book, J. Comput. Phys. **11**, 38 (1973).
- [9] G. Hazak, Phys. Plasmas **9**, 345 (2002).
- [10] M. Klapisch *et al.*, Phys. Plasmas **5**, 1919 (1998); A. Bar-Shalom *et al.*, J. Quant. Spectrosc. Radiat. Transfer **71**, 169 (2001).
- [11] C.J. Pawley *et al.*, Phys. Plasmas **6**, 565 (1999).
- [12] Y. Aglitskiy *et al.*, Phys. Plasmas **9**, 2264 (2002).
- [13] D.G. Colombant *et al.*, Phys. Plasmas **7**, 2046 (2000).
- [14] R.W. Lee and J.T. Larsen, J. Quant. Spectrosc. Radiat. Transfer **56**, 535 (1996).
- [15] O. Peyrusse, J. Quant. Spectrosc. Radiat. Transfer **51**, 281 (1994).
- [16] M. Busquet *et al.*, J. Quant. Spectrosc. Radiat. Transfer **71**, 225 (2001).
- [17] S.P. Obenschain *et al.*, Phys. Plasmas **3**, 2098 (1996).
- [18] R.H. Lehmsberg and S.P. Obenschain, Opt. Commun. **46**, 27 (1983).
- [19] J.L. Weaver *et al.*, Phys. Plasmas **8**, 5230 (2001).
- [20] W.E. Behring *et al.*, Appl. Opt. **27**, 2762 (1988).
- [21] R.E.H. Clark *et al.*, Astrophys. J. **254**, 412 (1982); R.E.H. Clark *et al.*, Astrophys. J. Suppl. Ser. **49**, 545 (1982); S.J. Goett, D.H. Sampson, At. Data Nucl. Data Tables **29**, 535 (1983); S.J. Goett *et al.*, At. Data Nucl. Data Tables **28**, 279 (1983); V.L. Jacobs and M. Blaha, Phys. Rev. A **21**, 525 (1980); A.K. Pradhan *et al.*, Astrophys. J. **246**, 1031 (1981); L.A. Vainshtein and U.I. Safranova, At. Data Nucl. Data Tables **25**, 49 (1978); D.H. Sampson *et al.*, At. Data Nucl. Data Tables **28**, 299 (1983); D.H. Sampson and H.L. Zhang, Astrophys. J. **335**, 516 (1988); A.V. Vinogradov *et al.*, Sov. J. Quantum Electron. **5**, 630 (1975).
- [22] D. Gilles and O. Peyrusse, J. Quant. Spectrosc. Radiat. Transfer **53**, 647 (1995).